Ultrafast Dynamics of Gold-Based Nanocomposite Materials†

ARTICLE *in* THE JOURNAL OF PHYSICAL CHEMISTRY A · APRIL 2003

Impact Factor: 2.69 · DOI: 10.1021/jp026885d

3 AUTHORS, INCLUDING:

Valeria Kleiman
University of Florida
50 PUBLICATIONS **1,442** CITATIONS

SEE PROFILE

Ultrafast Dynamics of Gold-Based Nanocomposite Materials†

Joseph S. Melinger,* Valeria D. Kleiman,‡ and Dale McMorrow

Naval Research Laboratory, Electronics Science and Technology Division, Code 6812, Washington, D.C. 20375

Franziska Gröhn,§ Barry J. Bauer, and Eric Amis

Polymers Division, National Institute of Standards and Technology, Gaithersburg, Maryland 20899

Received: August 30, 2002; In Final Form: February 28, 2003

Ultrafast electron dynamics are compared for small (2.5- to 4.0-nm average diameter) Au nanoparticles in two different surrounding environments. In one case, an aqueous solution contains Au nanoparticles (with average diameters of either 2.5 or 4.0 nm) embedded inside polyamidoamine (PAMAM) dendrimers. In the other case, hexanethiol-passivated (HT) Au nanoparticles, with an average diameter of 3.6 nm, are suspended in dichloromethane solution. Femtosecond two-color pump−probe spectroscopy is used to excite and probe the dynamics of the Au nanoparticles in the region of the surface plasmon resonance. The transient response is measured as a function of laser excitation fluence (J/cm^2). For the metal−dendrimer nanocomposites, the transient response consists of a single-exponential decay that relaxes with a time constant of less than 1.2 ps and is due mainly to electron−phonon coupling. The relaxation time scale shows a weak dependence on excitation fluence but is essentially independent of the size of the Au nanoparticle embedded inside the dendrimer (for the size range investigated). In contrast to the metal−dendrimer systems, the transient response of the Au-HT in dichloromethane reveals both electron−phonon and phonon−phonon relaxation components, and the relaxation time scale shows a relatively stronger dependence on excitation fluence. A qualitative discussion is given for the different relaxation characteristics that are observed for the two Au nanoparticle systems.

Introduction

The linear and nonlinear optical properties of organic−inorganic hybrid materials are presently topics of intense interest. New methods of macromolecular synthesis and molecular engineering allow the fabrication of hybrid materials consisting of organic macromolecules that are attached to, or even contain, semiconductor or metallic nanoparticles.[1−4] The prospect of controlling the optical properties of such materials gives them significant potential for technological applications. From a more fundamental perspective, hybrid materials present a fascinating medium with which to explore photophysical phenomena.

In this paper, we investigate the ultrafast dynamics of small (2.5- to 4.0-nm average diameter) Au nanoparticles contained in two different types of environments. In the first case, the Au nanoparticles are embedded inside polyamidoamine (PAMAM) dendrimers and suspended in aqueous solution. A schematic representation of this system is shown in Figure 1. Because of the strong optical absorption due to the surface plasmon resonance, metal−dendrimer nanocomposites have potential applications in optoelectronics, and reports have recently appeared on their time-dependent emission[5a] and nonlinear optical properties.[5b] In the second case, similar-sized Au nanoparticles (average diameter = 3.6 nm) are passivated by hexanethiol molecules and suspended in dichloromethane solvent. Comparing the ultrafast optical response of these two systems provides insight into how the hot electron dynamics of small metal nanoparticles depend on the structural and thermodynamic properties of the surrounding medium.

Dendrimers have been shown to incorporate molecules,[6,7] and even nanometer-sized metal colloids,[1] into their interiors. Recently, it has been demonstrated that PAMAM dendrimers can be used as a template to synthesize metal colloids in an aqueous environment.[1−4] For smaller-generation PAMAM dendrimers ($g \leq 6$, where g is generation), the nanoparticle is thought to be stabilized in solution with several PAMAMs forming a shell around the surface of the metal nanoparticle.[1,2] For larger-generation PAMAM dendrimers ($g > 6$), it has been shown that the metal nanoparticle can form inside the dendrimer interior, leading to the "caged" structure referred to above.[1] The dendrimer template restricts the Au particle size, leading to an ensemble of Au particles with a well-defined size.[1] Furthermore, the dendrimer serves as a passivating medium to prevent the aggregation of the metal colloids, which permits the optical and nonlinear optical properties of individual nanoparticles to be characterized at much higher concentrations than are possible without the cage. There is also the issue of what role the PAMAM dendrimer cage plays in the dissipation of excess energy from a metal nanoparticle to its surroundings. Since H_2O molecules penetrate the PAMAM dendrimer in an aqueous environment, both surrounding materials can affect the time-dependent optical response of the Au nanoparticle. Probing the metal nanoparticle using ultrafast spectroscopy can provide

† Part of the special issue "George S. Hammond & Michael Kasha Festschrift".

* Corresponding author. E-mail: melinger@ccf.nrl.navy.mil.

‡ Department of Chemistry, University of Florida, Gainesville, Florida.

§ Current Address: Max-Planck-Institut für Polymerforshung, Ackermannweg 10, D-55128, Mainz, Germany.

10.1021/jp026885d CCC: $25.00
Published on Web 05/01/2003

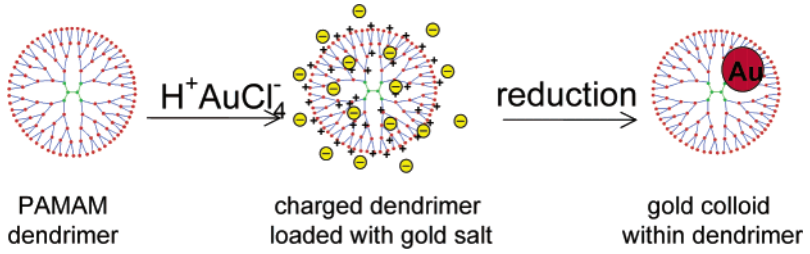

Figure 1. Schematic representation of the templating of a Au nanoparticle in a PAMAM dendrimer in aqueous solution. After the reduction of the charged dendrimer solution, the Au nanoparticle is located offset from the center of the PAMAM dendrimer.

valuable information regarding the nanoparticle/dendrimer environment.

The hot electron dynamics of Au nanoparticles as colloids in solution, or embedded within solid-state dielectric materials, have received considerable attention,[8−18] and much has been learned about the relaxation mechanisms that return the non-Fermi electron distribution back to equilibrium. Following ultrashort pulsed-laser excitation, the non-Fermi distribution initially relaxes through electron−electron and electron−phonon relaxation steps, which lead to the excitation of the metal lattice (phonons). A somewhat less detailed picture is available for the final relaxation step where excess energy is transferred to the surrounding medium.[8,11,12a,18]

In this paper, the hot electron dynamics are characterized using femtosecond two-color pump−probe spectroscopy. The different Au nanocomposites are excited and probed in the spectral region of the surface plasmon resonance (SPR), and the Au nanoparticle electron dynamics are measured over a range of excitation fluences. For excitation fluences up to 800 μJ/cm^2 the dendrimer-encapsulated Au nanoparticles exhibit a transient bleach response that is characterized by a single-exponential relaxation component, due primarily to electron−phonon coupling. The relaxation time constant is found to depend weakly on the excitation fluence. For all values of excitation fluence, the characteristic relaxation time is less than 1.2 ps. Furthermore, at a given excitation fluence, the relaxation time is found to be independent of the diameter of the Au nanoparticle for the size range investigated. In contrast, over the same range of excitation fluences, the hexanethiol-passivated Au nanoparticles suspended in dichloromethane exhibit a significantly steeper fluence dependence of the electron−phonon relaxation time constant. In addition, the hexanethiol-passivated Au nanoparticles reveal a much longer time scale (>20 ps) relaxation component, which is largely absent in the dendrimer-encapsulated nanoparticles. A qualitative discussion is given for the different relaxation characteristics that are observed for the two Au nanoparticle systems.

Experimental Section[28]

The synthesis of the dendrimer-encapsulated Au nanoparticles has been described previously.[1] Briefly, aqueous solutions of g7 and g9 PAMAM dendrimers (0.1 to 1.0% mass fraction) were mixed with stoichiometric amounts of an aqueous $HAuCl_4$ solution. The formation of colloids within the PAMAM matrix was induced by adding the reducing agent $NaBH_4$ in basic aqueous solution. To control the nanoparticle size, it is necessary to optimize the Au/dendrimer ratio, and details for the optimization of the Au/dendrimer ratio are provided in ref 1. The hexanethiol-passivated Au nanoparticles were prepared by the method given in ref 19.

The colloidal Au solutions were characterized by a variety of techniques. The UV−vis absorption spectra were obtained using a Perkin-Elmer Lambda-9 spectrometer.[3] Structural information regarding the average diameter of the Au radii, the average diameter of the dendrimer, and the placement of the Au nanoparticle inside the PAMAM dendrimer was obtained from transmission electron microscopy (TEM), small-angle neutron scattering (SANS), and small-angle X-ray scattering (SAXS). The details of these measurements are given in ref 1.

The ultrafast dynamics measurements were performed using an apparatus based on a kilohertz regeneratively amplified titanium sapphire laser, which produces intense laser pulses centered at 790 nm with a pulse width of about 120 fs at the fwhm, as determined from autocorrelation measurements. Pump pulses were obtained from an optical parametric amplifier (OPA) pumped by the main portion of the amplified Ti:sapphire output. The output of the OPA was frequency doubled using a β-barium borate crystal to yield pulses of approximately 150 fs duration at the fwhm at a central wavelength of 600 nm. Probe pulses were generated by focusing a small portion of the amplified Ti:sapphire beam (approximately 1 to 2%) onto a 1-mm sapphire plate to produce a single-filament white-light continuum. The instrument response was measured by cross correlation of the pump and probe in a 1-mm ZnS plate and was typically between 240 and 300 fs at the fwhm. Nondegenerate pump−probe experiments were performed with parallel pump and probe polarizations. The pump beam was gently focused to a $1/e^2$-radius spot of approximately 150 μm while the probe was focused more tightly to a $1/e^2$-radius spot of approximately 100 μm and spatially overlapped with the pump spot. The spot radii of the pump and probe were estimated by translating a razor blade through the beam at the point where the beams entered the sample. A 1-mm path length cell was used with the sample at an optical density near 0.5 at 520 nm. The transmitted probe beam was passed through a narrow band-pass filter centered near 520 nm. A portion of the probe was passed through the sample below the pump beam and was used as a reference beam to remove the pulse-to-pulse energy fluctuations. Both transmitted (probe and reference) beams were detected by photodiodes and integrated by a boxcar averager. The experiments were conducted at repetition rates ranging from 50 Hz to 1 kHz.

Uncertainties listed in this paper represent one standard deviation in the absolute value. Values of the particle size, laser fluence, and energies have standard uncertainties of approximately 10−15% of the listed values based on previous experience with such measurements. Concentrations and wavelengths have standard uncertainties of approximately 10% of the listed values based on previous experience with such measurements. The standard deviations shown in the figures are plotted when they exceed the plotting symbol size but are left out for simplicity when the values are smaller.

Results and Discussion

A. Sample Characterization. The formation of the dendrimer-encapsulated nanoparticles is illustrated schematically

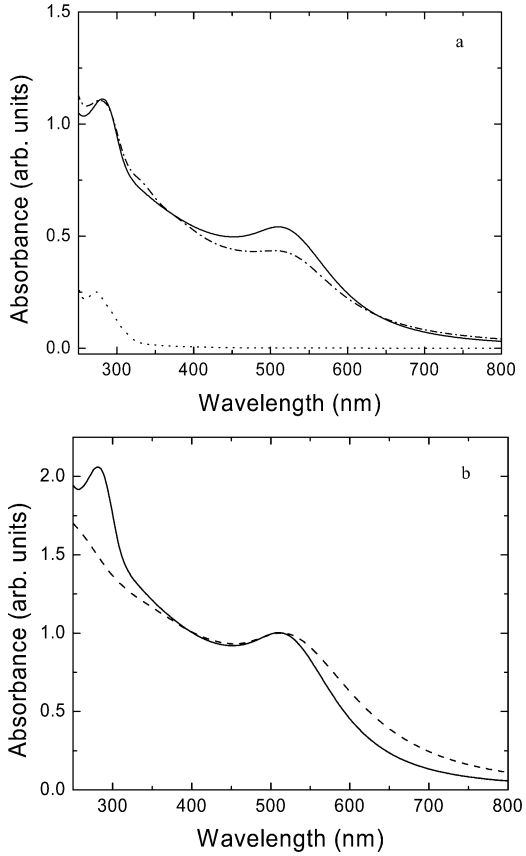

Figure 2. Absorption spectra of Au-PAMAMs and Au-HT. (a) Absorption spectra of Au(g7) (− · −) and Au(g9) nanocomposites (—) and an unoccupied g9 PAMAM dendrimer in H_2O (···). (b) Comparison of the absorption spectra of Au-HT (− − −) with Au(g9)-PAMAM (—).

in Figure 1. Initially, an aqueous solution of dendrimer is charged with $H^+(AuCl_4)^-$ salt. A stable Au colloid is formed inside the larger-diameter dendrimer upon reduction of the gold salt with $NaBH_4$. Characterization of the composite with SANS and SAXS showed that one Au colloid forms inside the dendrimer and that its location is offset from the center of the dendrimer for g7 and g9.[1] A combination of TEM, SANS, and SAXS measurements showed that the average colloid diameters R are 2.5 and 4.0 nm; these colloids are embedded in the g7 and g9 PAMAMs, respectively. The size distribution of the Au diameter is approximately ±10%. The relative theoretical molecular masses of the PAMAMs are 116 344 and 467 546 g/mol for g7 and g9, respectively. The relative molecular masses of the encapsulated Au nanoparticles can be estimated by using the density of bulk gold (19.3 g/mL) and are 95 000 (R = 2.5 nm) and 390 000 (R = 4.0 nm). Thus, for each nanocomposite, the relative mass of the PAMAM dendrimer is somewhat greater than the (estimated) relative mass of the encapsulated Au. For the hexanethiol-passivated Au colloids, the average diameter is 3.6 nm with a size distribution of ±15−20%.

B. Steady-State Spectroscopy. Figure 2a shows the absorption spectra for the Au(g7, g9) PAMAMs at 298 K. The spectral characteristics in the SPR region for each of the Au nanoparticles are summarized in Table 1. In each case, the absorption spectrum reveals a broad peak with a maximum near 510 nm that is due to the surface plasmon resonance (SPR) and a rising shoulder to the blue of the plasmon resonance that is due to interband transitions in gold. The HWHM widths of the SPRs (measured from the peak to the red side of the SPR) are 0.38 eV (2830 cm^{-1}) and 0.32 eV (2550 cm^{-1}) for the g7 and g9 Au/PAMAMs, respectively. The dotted line is the absorption spectrum of a g9 PAMAM in H_2O without any Au present. The PAMAM dendrimer has negligible absorption in the region of the Au SPR but exhibits a weak tail that begins at wavelengths near 400 nm. There is a weak peak near 270 nm that precedes the onset of a stronger absorption due to the dendrimer, which begins near 250 nm. Although deviations from spherical particles and a 10−15% size distribution can affect the optical properties of the Au SPR, we find that the peak position and spectral width of the Au-PAMAM SPRs are similar to those of other Au nanoparticles in aqueous environments.[12]

TABLE 1: Energy and Spectral Width of the Surface Plasmon Resonance for Each of the Au Nanoparticle Systems

	diameter (nm)	maximum (eV)	HWHM spectral width (eV)
Au(g9)-PAMAM	4.0	2.43 (510 nm)	0.32
Au(g7)-PAMAM	2.5	2.47 (502 nm)	0.38
Au-HT	3.6	2.41 (514 nm)	0.42

Figure 2b compares the absorption spectra of the Au(g9)-PAMAM with HT-passivated Au nanoparticles in dichloromethane solution (Au-HT). The HWHM of the SPR for Au-HT is 3420 cm^{-1} (0.42 eV), which is significantly larger than the spectral HWHM for Au(g9)-PAMAM. The spectral characteristics of Au-HT are similar to those of other alkanethiol-passivated Au nanoparticles.[13,20] The increased broadening exhibited by Au-HT relative to Au(g9)-PAMAM is due to a smaller average particle size and, possibly, a larger size distribution. The adsorption of the thiol groups at Au sites may also affect the width of the SPR.[20]

It is useful to examine whether a more quantitative analysis of the SPR for the metal−dendrimer nanocomposites can be obtained using Mie scattering theory. The modeling of the Au SPR is also useful in estimating of the initial temperature rise induced by ultrashort pulsed-laser excitation. For metal particles much smaller than the wavelength of the excitation light, the absorption cross section can be approximated by the dipole term of the Mie equation[21]

$$\sigma(\omega) \propto \frac{\epsilon_2(\omega)}{[\epsilon_1(\omega) + 2\epsilon_m]^2 + [\epsilon_2(\omega)]^2} \tag{1}$$

where $\epsilon_1(\omega)$ and $\epsilon_2(\omega)$ are the real and imaginary parts, respectively, of the dielectric constant for the absorbing metal particle, ϵ_m is the dielectric constant of the surrounding medium, and ω is the frequency of the incident light. The complex dielectric function for the metal particle is written as

$$\epsilon(\omega) = \epsilon_D(\omega) + \epsilon_{IB}(\omega) \tag{2}$$

where $\epsilon_D(\omega)$ is the free-electron (Drude) contribution

$$\epsilon_D(\omega) = 1 - \frac{\omega_p^2}{\omega(\omega - i\Gamma)} \tag{3}$$

and $\epsilon_{IB}(\omega)$ is the contribution due to interband transitions. In eq 3, ω_p is the plasmon frequency of the free electrons, and Γ is the damping constant associated with the electron's mean free path. To model the interband contribution, we follow the procedure used in refs 9 and 11, where

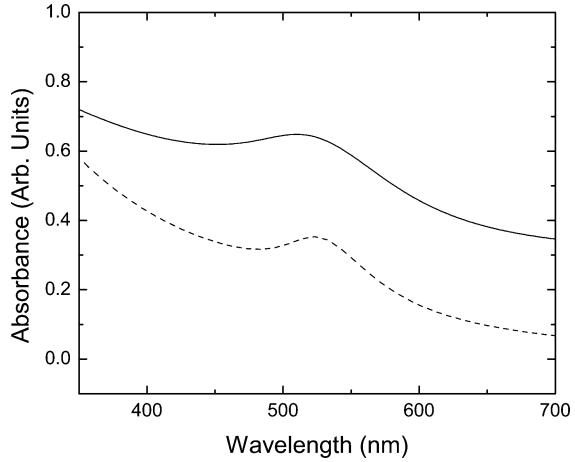

Figure 3. Experimental (—) and calculated (– – –) absorption spectra. Both spectra correspond to the case of Au(g9)-PAMAM.

$$\epsilon_{IB}(\omega) \propto \frac{1}{\omega^2}\int_{\omega_g}^{\infty}\frac{\sqrt{x-\omega_g}}{x}[1-F(x,\Theta_e)]\times \left(\frac{\omega^2-x^2-\gamma_{ee}{}^2-2i\omega\gamma_{ee}}{(\omega^2-x^2-\gamma_{ee}{}^2)^2+4\omega^2\gamma_{ee}{}^2}\right)dx \quad (4)$$

In eq 4, F is the Fermi distribution function at an electron temperature Θ_e, ω_g is the band-gap energy, and γ_{ee} is the damping constant for the band-to-band transition.

Figure 3 shows a calculated absorption spectrum for the case of Au(g9)-PAMAM using eqs 1−4. In the calculation, ω_g = 1.7 eV, Θ_e = 298 K, and ω_p = 8.9 eV.[20] Since the contribution to the dielectric constant of the surroundings by the dendrimer is unknown, we approximate ϵ_m by using the dielectric constant of H_2O, or $2\epsilon_m$ = 3.55 at 298 K.[21] The calculated absorption spectrum was obtained with Γ = 0.75 eV and γ_{ee} = 0.13 eV. The calculation only roughly reproduces the features of the experimental absorption spectrum. The calculated position of the SPR peak appears at about 10 nm to the red side of the experimental SPR peak, and the calculation significantly underestimates the width of the experimental SPR. Attempts to calculate the spectral features of the other nanocomposite samples yielded similar discrepancies. Some of the extra broadening in the experimental absorption spectrum is likely due to the distribution of particle sizes in the sample, which is not considered in the calculation. The discrepancies between the experimental and calculated absorption spectra are similar to those found in previous attempts to calculate the absorption spectra of very small Au nanoparticles using Mie theory.[20]

C. Transient Pump−Probe Dynamics. Figure 4a−c shows the ultrafast transient pump−probe data for each of the nanoparticle systems as a function of excitation fluence, which ranged from 100 to 800 μJ/cm^2. In each case, the central laser pump wavelength was 600 nm, and the central wavelength of the probe was tuned to near the peak region of the SPR. Figure 4a and b shows the transient bleach response of the Au-PAMAMs, and Figure 4c shows the transient bleach response of the Au-HT. The *y*-axis represents the normalized change in sample transmission $\Delta T/T$, or $(T_f - T_i)/T_i$ where T_f represents the probe pulse fluence transmitted through the sample and T_i represents the incident probe pulse fluence.

Figure 5 shows the fluence dependence of the change in sample transmission measured near the peak. In each case, the peak signal shows a near-linear dependence on the excitation fluence. At a given excitation fluence, the peak signal also

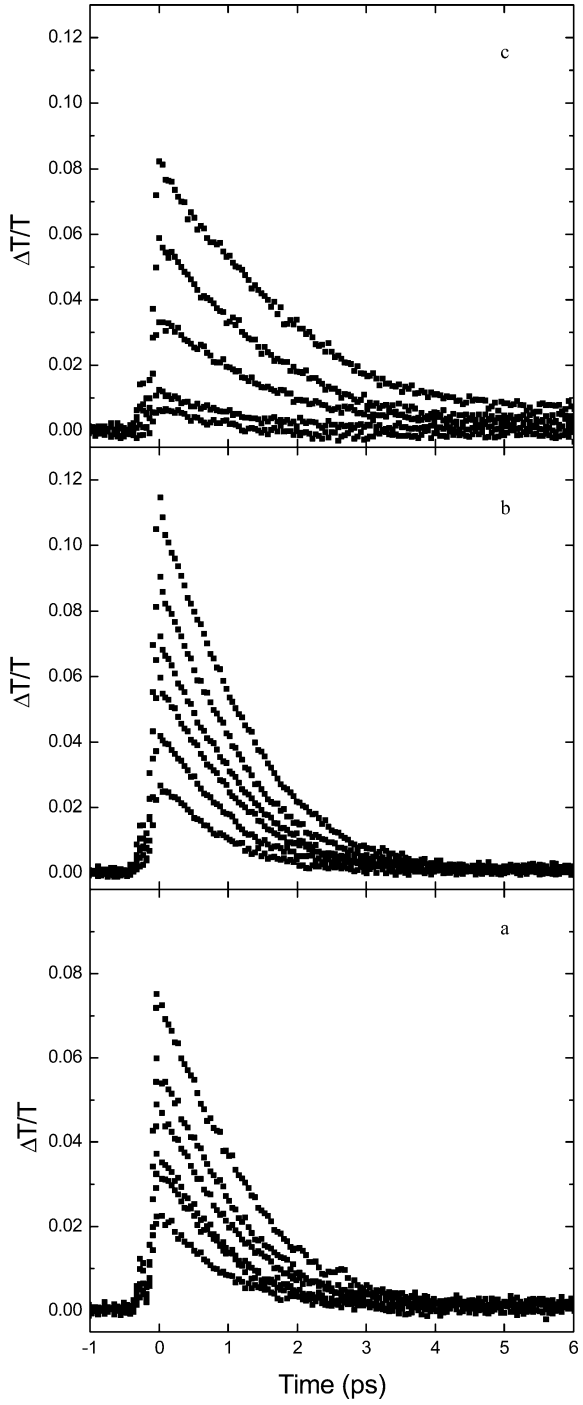

Figure 4. Transient bleach response for Au-PAMAMs and Au-HT as a function of excitation fluence. (a) Au(g7), (b) Au(g9), (c) Au-HT. From bottom to top of each graph in a−c, the excitation fluence corresponds to 100, 200, 300, 400, 500, 600, and 800 μJ/cm^2.

increases with increasing nanoparticle diameter. The magnitude of the induced transmission is related to the change in the absorption cross section of the nanoparticles

$$\frac{\Delta T}{T} = \exp(-[\sigma(\omega,\Theta_e) - \sigma(\omega,\Theta_e = 298\text{ K})]NL) - 1 \quad (5)$$

where N is the sample number density and L is the path length. Equations 1−5 can be used to estimate the initial elevated electron temperature. This calculation was performed for Au(g9)-PAMAM. At the highest applied laser fluence (800 μJ/cm^2), the initial electron temperature is estimated to be approximately 1100 K.

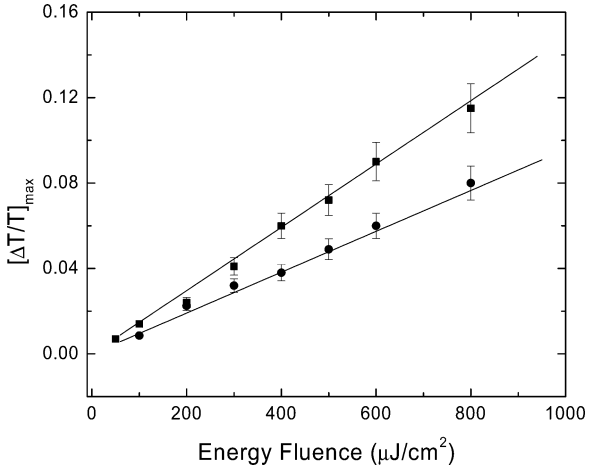

Figure 5. Dependence of the peak transient bleach signal (around $t = 0$) vs excitation fluence. ● = Au(g7), ■ = Au(g9). The solid lines represent linear fits to the data.

The transient bleach signals corresponding to Au-PAMAMs (Figure 4a and b) show primarily a single rapidly relaxing component that recovers to equilibrium in less than 5 ps. Furthermore, the time constant for the transient bleach signal increases with pump fluence. For the same range of excitation fluence, the transient bleach signals for the Au-HTs exhibit somewhat different characteristics (Figure 4c). Here, the signal exhibits the rapid picosecond-time-scale component found in the Au-PAMAMs; however, there is a larger change in the relaxation times over the same range of excitation fluence. Furthermore, the Au-HT transients also show a residual component that relaxes with a time constant that is greater than 20 ps. For each of the Au systems, the probe wavelength was varied by about ±10 nm near the SPR maximum, and only minor changes in the shape of the transient decays were observed. We note that for probe wavelengths farther from the peak region of the SPR, there can be significant changes in the shape of the transient signal due to shifting of the plasmon band.[9b,11−13] We also mention that two different sample preparations were measured for Au(g7)-PAMAM. Both preparations gave nearly identical dynamical measurements under the same conditions of incident pump fluence.

To quantify the relaxation times, the experimental transient bleach signals are fit to a convolution of the sum of a single-exponential decay function and a constant using a Gaussian function that approximates the instrumental response. The exponential time constants were determined through a Levenson−Marquardt fitting procedure. Representative fits for each of the samples are shown in Figure 6a−c, and the time constants are given in the caption.

D. Electron−Phonon Dynamics. The relaxation dynamics show features that are consistent with previous measurements of hot electron relaxation dynamics in noble-metal nanoparticle systems.[8−18] The initial non-Fermi electron distribution created by the ultrashort laser pump pulse relaxes primarily by electron−electron, electron−phonon, and phonon−phonon scattering processes. At short times, immediately following the laser pump pulse, electron−electron and electron−phonon scattering are the primary relaxation mechanisms. The time scale for electron−electron scattering depends on the excitation wavelength and is proportional to the square of the energy difference between the excited electrons and the Fermi level.[9,13b,c] For excitation of Au in the SPR region, the relaxation time due to electron−electron scattering occurs on a time scale of a few hundred femtoseconds.[13c,17] Since our experimental time resolution was not fast enough to resolve the electron−electron component, we consider only the electron−phonon and phonon−phonon mechanisms in the interpretation of the transients of Figure 4. We associate the fast component that relaxes on a time scale of 1 to 2 ps with the electron−phonon relaxation mechanism whereas the longer-lived (>20 ps) component is associated with the phonon−phonon relaxation.

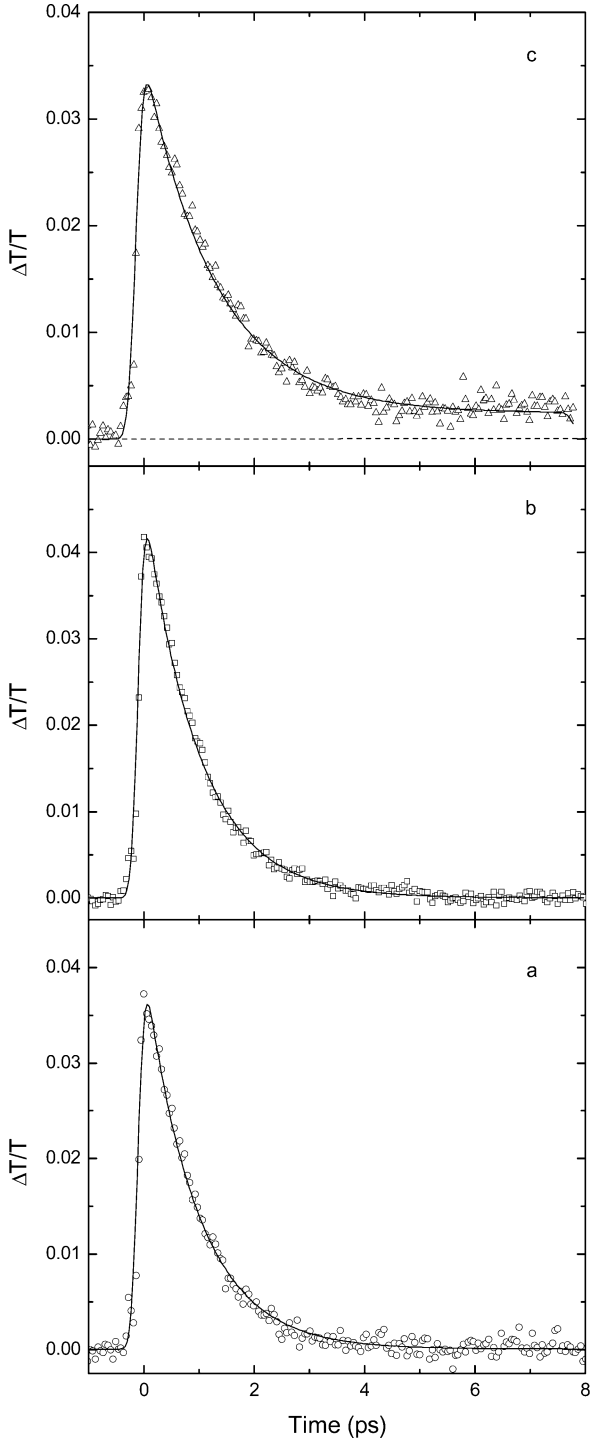

Figure 6. Fits of selected transient bleach signals to a convolution of an exponential decay function with the instrument response. The bleach responses (data points) and fits (solid lines) have been normalized and offset. (a) Au(g7), $F = 300$ μJ/cm^2, $\tau = 0.93$ ps, (b) Au(g9), $F = 400$ μJ/cm^2, $\tau = 0.95$ ps, (c) Au-HT, $F = 400$ μJ/cm^2, $\tau = 1.45$ ps.

The two-temperature model[22] has often been used to explain the time dependence of the transient bleach/absorption signals in thin metal films[23,24] and in metal nanoparticles.[11−13] The

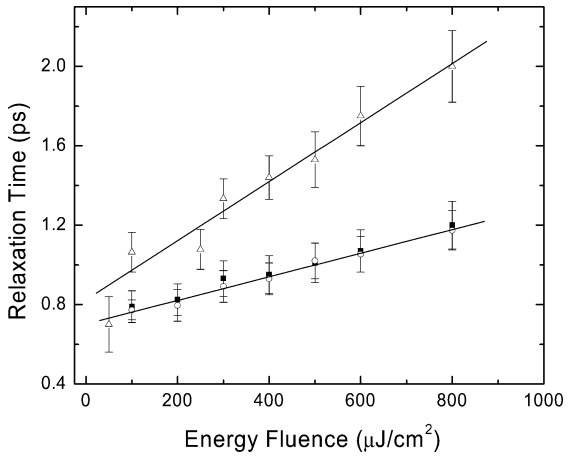

Figure 7. Electron−phonon relaxation time constants vs excitation fluence. ○ = Au(g7), ■ = Au(g9), △ = Au-HT. A linear fit to the data is shown for the cases of Au(g9) and Au-HT.

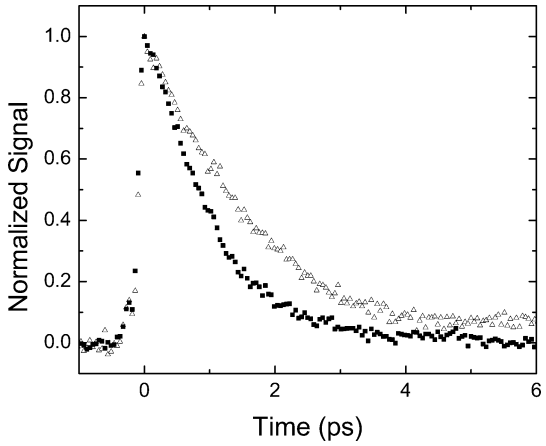

Figure 8. Comparison of the transient bleach signals for Au(g9) (■) and Au-HT (△) at an excitation fluence of 400 μJ/cm^2.

energy flow from the electron gas to the lattice is modeled by the following coupled differential equations:

$$C(\Theta_e)\frac{\partial\Theta_e}{\partial t} = -G(\Theta_e - \Theta_l) + P(t)$$
$$C_l\frac{\partial\Theta_l}{\partial t} = G(\Theta_e - \Theta_l) \quad (6)$$

In eq 6, Θ_e and Θ_l are the electron and lattice temperatures, respectively, and $C(\Theta_e) = \gamma\Theta_e$ is the electronic heat capacity, where $\gamma = 66$ J/m^3 K^2 for Au.[11] The constant G represents the electron−phonon coupling, and $P(t)$ represents the input power density. The relaxation of the electron temperature due to electron−phonon coupling is determined by the quantity $G/(\gamma\Theta_e)$. Thus, the electron−phonon relaxation time depends on the excitation fluence through the electron temperature.

One goal of this paper is to examine the effect of the surrounding medium on the hot electron dynamics of the Au nanoparticle. The fluence dependence of the electron−phonon relaxation time constants (determined by the fitting procedure) are plotted in Figure 7 and show that at a given excitation fluence the relaxation time constants corresponding to Au(g9)-PAMAM and Au-HT are different. To make this clearer, Figure 8 compares the Au(g9)-PAMAM and Au-HT transients measured at a laser excitation fluence of 400 μJ/cm^2. The transient bleach signal for the Au(g9)-PAMAM relaxes with a time constant of (0.95 ± 0.10) ps whereas Au-HT exhibits a

TABLE 2: Electron−Phonon Coupling Constants Obtained Using the Extrapolation Method for Each of the Au Nanoparticle Systems

	electron−phonon coupling, G ($\times 10^{16}$ W/m^{3}K)
Au(g9)-PAMAM	(2.7 ± 0.4)
Au(g7)-PAMAM	(2.8 ± 0.5)
Au-HT	(2.4 ± 0.5)

significantly longer initial decay time of (1.45 ± 0.12) ps as well as a long-lived component due to phonon−phonon coupling. One possibility for the longer relaxation time for Au-HT is that the incident laser fluence induces a much larger initial temperature rise. To check this, eqs 6 can be used to predict the initial electron temperature if the input energy density is known: $\int P(t)\,dt = (\sigma_{abs}F)/V$ where σ_{abs} is the absorption cross section, F is the incident fluence, and V is the nanoparticle volume. Previous experimental work has shown that σ_{abs} for Au nanoparticles is approximately one-half the physical cross section.[13b] Using this approximation to estimate σ_{abs} for Au particles studied here predicts an initial temperature ratio of $\Theta_{Au-HT}/\Theta_{Au-PAMAM} \cong 1.1$ (400 μJ/cm^2), which cannot account for the corresponding ratio of relaxation time constants: $\tau_{Au-HT}/\tau_{Au-PAMAM} \cong 1.5$ (400 μJ/cm^2).

The results shown in Figure 7 provide evidence that the surrounding medium can have a significant effect on the hot electron relaxation dynamics in Au nanoparticles. We note that a similar effect has been observed for silver nanoparticles (6.5-nm diameter) embedded in solid-state glass matrices of different thermal conductivities.[9b] In that study, the electron−phonon relaxation time was significantly faster for the nanoparticles embedded in the higher thermal conductivity matrix. For the systems studied here, there is a large difference in the thermal conductivity (κ) of the solvents dichloromethane ($\kappa = 0.137$ W/mK at 298 K) and H_2O ($\kappa = 0.607$ W/mK at 298 K). It is reasonable to assume that the larger thermal conductivity of H_2O is more effective in helping to cool the hot electron distribution, which would lead to a faster electron−phonon relaxation time in an aqueous surrounding medium relative to that in dichloromethane. In addition, we should consider the possibility that the dendrimer cage also plays a role in facilitating the relaxation of the hot electrons. The dendrimer framework can supply an additional manifold of states that may be effective in enhancing the electron−phonon coupling via a surface-mediated process. To better understand the role of the dendrimer cage, a direct experimental test such as probing for the appearance of excess vibrational energy in the PAMAM dendrimer following laser excitation of the Au nanoparticle must be devised.

If the initial electron temperature is known with certainty, then eqs 6 can be used to the estimate electron−phonon coupling constant G. Since it is difficult to know the precise initial electron temperature, a method has been suggested[12a] for estimating G by performing a series of power-dependent measurements and extrapolating the measured time constants to the low-power limit (i.e., $G = \gamma\Theta_o/\tau_o$ where Θ_o and τ_o represent room temperature and the relaxation time constant at room temperature, respectively). Figure 7 shows that the electron−phonon relaxation time constants for each of the Au-PAMAMs trend to similar limiting values at low power (about 725 fs at the y intercept). Table 2 summarizes the results of the extrapolation for each system. Each of the values for G is close to the bulk value for Au of (3.0 ± 0.5) × 10^{-16} W/m^{3}K.[25] The values in Table 2 imply that, to within our experimental resolution, for the Au-PAMAMs, there is not a strong size-

dependence for the electron−phonon coupling constant in the low-power limit. This observation is consistent with previous measurements on Au nanoparticles suspended in aqueous environments that showed no size dependence of G (in the low-power limit) in the size range from 2 to 30 nm.[12,13b] In contrast, the electron−phonon time constants for the Au-HTs appear to trend to a somewhat larger time constant at the low-power limit (about 825 fs). Although this result appears to suggest that there is a dependence of the electron−phonon coupling constant G on the surrounding medium, our experimental uncertainty is relatively large for the low-fluence measurements (approximately ±20%), thus there is a need to investigate the low-fluence region (<50 μJ/cm^2) with greater experimental sensitivity.

E. Phonon−Phonon Dynamics. The Au-PAMAM and Au-HT systems show different transient responses at times longer than a few picoseconds. The transient bleach signal of the Au-PAMAMs relaxes completely within 5 ps following the pump pulse (within our limits of sensitivity) for all values of the excitation fluence used in the experiment whereas the bleach signal for the Au-HTs reveals a long-lived component for all of the excitation fluences above 100 μJ/cm^2. This difference in the long-time behavior suggests that the phonon−phonon coupling for the two systems is stronger for the Au-PAMAMs. The phonon−phonon relaxation has been modeled by considering the thermal diffusion from the Au lattice to the surrounding medium according to the diffusion equation[11,18]

$$\frac{\partial \Theta_{\mathrm{surr}}}{\partial \tau} = D_{\mathrm{surr}} \nabla^2 \Theta_{\mathrm{surr}} \tag{7}$$

and by requiring energy uniformity across the interface between the nanoparticle and the surrounding medium,[11,18]

$$C_{\mathrm{l}} V \Theta_{\mathrm{l,init}} = C_{\mathrm{l}} V \Theta_{\mathrm{l}}(t) + C_{\mathrm{surr}} \int_{r=R/2}^{\infty} 4\pi r^2 \, \Delta\Theta_{\mathrm{surr}}(t, r) \, \mathrm{d}r \tag{8}$$

In eq 7, Θ_{surr} and D_{surr} are the temperature and the thermal diffusivity of the surrounding medium, respectively. In eq 8, C_{l} is the lattice heat capacity, C_{surr} is the heat capacity of the surroundings, and V is the nanoparticle volume and R is its diameter. Equations 7 and 8 have been solved analytically for the time dependence of the lattice temperature, and the solution is given in ref 11 as eq 10. At short times (near $t = 0$), the normalized change in lattice temperature is approximated by

$$\frac{\Theta_{\mathrm{l}}(t) - 298\ \mathrm{K}}{\Theta_{\mathrm{l}}(0) - 298\ \mathrm{K}} \cong 1 - \left[\left(\frac{24 D_{\mathrm{surr}}}{R^2}\right)\left(\frac{C_{\mathrm{surr}}}{C_{\mathrm{l}}}\right)\right] t$$

Clearly, smaller diameter particles, larger thermal diffusivities, and larger heat capacities favor a faster initial relaxation of the lattice temperature. Figure 9 shows the calculated time dependence of the normalized change in the Au lattice temperature (using eq 10 of ref 11) for an H_2O environment and a dichloromethane environment. The calculation is performed using the bulk solvent values for D_{surr} and C_{surr} (at 298 K): $D_{H_2O} = 1.45 \times 10^{-3}$ cm^2/s and $D_{CH_2Cl_2} = 7.67 \times 10^{-4}$ cm^2/s; $C_{H_2O} = 4.18 \times 10^6$ J/m^{3}K and $C_{CH_2Cl_2} = 1.56 \times 10^6$ J/m^{3}K. Both calculated transients show a rapid initial relaxation of the lattice temperature that is followed by a slower relaxation. At long times, the calculation predicts a relatively higher lattice temperature for the Au nanoparticles in dichloromethane than in H_2O, which is consistent with the presence of the long-lived component in the experimental Au-HT transients and its absence in the Au-PAMAM transients. The results here may be contrasted with vibrational relaxation in molecular liquids. We note that the solvent environment can significantly affect vibrational relaxation times (T_1). For example, the T_1 lifetime of an OH stretch in liquid H_2O is less than 1 ps[26] whereas in a CCl_4 environment the T_1 lifetime for an OH stretch is typically much longer, 10−100 ps.[27]

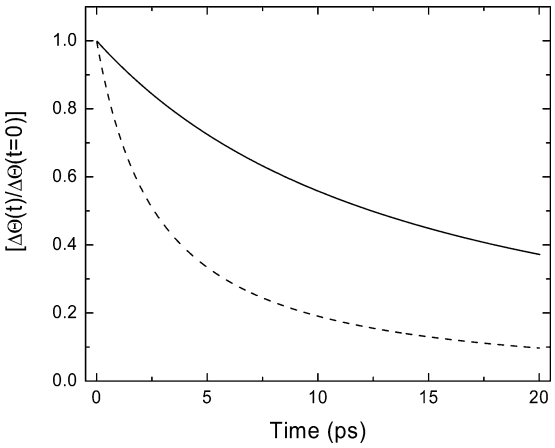

Figure 9. Comparison of the normalized change in the Au lattice temperature as calculated from equation 10 in reference 11 for an H_2O environment (—), and a dichloromethane environment (− − −).

In an attempt to isolate the role of the PAMAM dendrimer in the Au lattice relaxation, we performed pump−probe experiments on a dilute aqueous solution of Au nanoparticles (average diameter = 5.0 nm, optical density approximately 0.075 in a 1-mm path) obtained from a commercial source. For this sample, a long-lived component was observed in the transient bleach signal for excitation fluences above 200 μJ/cm^2. When compared to the case of the dendrimer-encapsulated Au, this result appears to provide evidence that the PAMAM dendrimer plays a role in facilitating the rapid removal of excess energy from the nanoparticle. However, because the Au nanoparticles from the commercial source were not made by the same method as that used to synthesize the dendrimer-encapsulated nanoparticles, other factors related to the fabrication of the samples must be considered. For example, thermal desorption of anions from the surface of an Au nanoparticle has been invoked as a mechanism that could give rise to a long-lived transient.[12a] The anionic species and ionic strength of the commercial sample and the Au-PAMAMs investigated here are different, thus thermal desorption cannot be ruled out as a mechanism giving rise to the long-lived component in the transient bleach signal of the commercially obtained Au solution.

Summary and Conclusions

In this paper, we have investigated the ultrafast dynamics of novel dendrimer-encapsulated Au nanoparticles. Each of the different-sized Au-PAMAMs exhibits an ultrafast transient bleach response that is characterized by a single-component exponential decay with a time constant of less than 1.2 ps. The relaxation dynamics are attributed to electron−phonon coupling, and its corresponding relaxation time shows a weak dependence on excitation fluence. Using the extrapolation method of ref 12, the electron−phonon coupling constant is estimated for each of the Au-PAMAMs and is found to approach the value for bulk Au, which is consistent with previous results that showed that there is not a strong size dependence for the electron−phonon coupling constant.[12,13] Our results confirm that the

dendrimer cage, at the very least, provides a stable passivating environment for the Au nanoparticles; however, the role that the PAMAM cage plays in the relaxation dynamics is not fully established. Although it is possible that the extra manifold of vibrational states provided by the PAMAM can serve as a channel for electron−phonon and/or phonon−phonon relaxation, more work must be done to reach a firm conclusion. One approach to address this issue would be to investigate the same metal−dendrimer nanocomposites in a suitable solvent that has significantly different thermodynamic properties relative to those of H_2O.

The ultrafast relaxation dynamics of the similar-sized Au nanoparticles passivated by hexanethiol molecules and suspended in dichloromethane were also investigated and compared to the dynamics of Au-PAMAMs at identical values of excitation fluence. In contrast to the Au-PAMAMs, the Au-HT system exhibits both electron−phonon and phonon−phonon relaxation components in its transient bleach response. The electron−phonon relaxation time constant shows a significantly steeper dependence on excitation fluence than do the Au-PAMAMs, which provides evidence that that the surrounding medium plays a role in the electron−phonon coupling. The presence of an additional slowly relaxing component in the Au-HT transient bleach response and its absence in the response of the Au-PAMAMs are consistent with the smaller thermal conductivity of dichloromethane relative to that of H_2O, which leads to less efficient phonon−phonon coupling in the Au-HT system.

Finally, we mention the possibility that adsorbed alkanethiol may play a role in mediating the transient bleach response of the Au-HT system. To understand the role of the surroundings for the Au-HT more thoroughly, it will be useful to perform pump−probe experiments for different chain length alkanethiols while keeping the solvent fixed and comparing to the case where the solvent is changed while keeping the alkanethiol the same.

Acknowledgment. This work was supported by the Office of Naval Research. F.G., B.J.B., and E.A. thank the U.S. Army Research office for partial support under contract number 35109-CH and Donald Tomalia of MMI for providing us with dendrimers. J.S.M thanks Art Snow of NRL for providing hexanethiol-capped Au nanoparticles.

References and Notes

(1) Gröhn, F.; Bauer, B. J.; Akpalu, Y. A.; Jackson, C. L.; Amis, E. A. *Macromolecules* **2000**, *33*, 6042.

(2) (a) Esumi, K.; Suzuki, A.; Aihara, N.; Usui, K. Torigo, K.; *Langmuir* **1998**, 14, 3157. (b) Esumi, K.; Suzuki, A.; Yamahira, A.; Torigoe, K. *Langmuir* **2000**, *16*, 2000.

(3) (a) Balogh, L.; Tomalia, D. A. *J. Am. Chem. Soc*. **1998**, *120*, 7355. (b) Balogh, L.; Valuzzi, R.; Laverdure, K. S.; Gido, S. P.; Hagnauer, G. L.; Tomalia, D. A. *J. Nanopart. Res.* **1999**, *1*, 353.

(4) Sooklal, K.; Hanus, L. H.; Ploehn, H. J.; Murphy, C. J. *Adv. Mat*. **1998**, *10*, 1083.

(5) (a) Varanavski, O.; Ispasoiu, R. G.; Balogh, L.; Tomalia, D.; Goodson, T., III *J. Chem. Phys.* **2001**, *114*, 1962. (b) Ispasoiu, R. G.; Balogh, L.; Varanavski, O.; Tomalia, D.; Goodson, T., III. *J. Am. Chem. Soc*. **2000**, *122*, 11005.

(6) Meyer, B.; Jansen, J. F. G. A.; deBrabander-van den Berg, E. M. M.; Meijer, E. W. *Science (Washington, D.C.)* **1994**, *266*, 1226.

(7) Kleinman, M. H.; Flory, J. H.; Tomalia, D. A.; Turro, N. J. *J. Phys. Chem. B* **2000**, *104*, 11472.

(8) Heilweil, E. J.; Hochstrasser, R. M. *J. Chem. Phys*. **1985**, *82*, 4762.

(9) (a) Bigot, J.-Y.; Merle, J.-C.; Cregut, O.; Daunois, A. *Phys. Rev. Lett*. **1995**, *75*, 4702. (b) Bigot, J.-Y.; Halte, V.; Merle, J.-C.; Daunois, A. *Chem. Phys*. **2000**, *251*, 181.

(10) Perner, M.; Bost, P.; Lemming, U.; Von Lessen, G.; Feldmann, J.; Becker, U.; Manning, M.; Schmitt, M.; Schmitt, H. *Phys. Rev. Lett*. **1997**, *78*, 2192.

(11) Inouye, H.; Tanaka, K.; Tanahishi, I.; Kazayuki, H. *Phys. Rev. B.* **1998**, *57*, 11334.

(12) (a) Hodak, J.; Martini, I.; Hartland, G. V. *J. Phys. Chem. B* **1998**, *102*, 6958. (b) Hodak, J.; Henglein, A.; Hartland, G. V. *J. Chem. Phys*. **2000**, *112*, 5942. (c) Hodak, J.; Henglein, A.; Hartland, G. V. *J. Phys. Chem. B* **2000**, *104*, 9954.

(13) (a) Logunov, S. L.; Ahmadi, T. S.; El-Sayed, M. A.; Khoury, J. T.; Whetten, R. L. *J. Phys. Chem. B* **1997**, *101*, 3713. (b) Link, S.; El-Sayed, M. A. *J. Phys. Chem. B* **1999**, *103*, 8410. (c) Link, S.; Burda, C.; Wang, Z. L.; El-Sayed, M. A. *J. Chem. Phys*. **1998**, *111*, 1255.

(14) Hache, F.; Ricard, D.; Flytzanis, C.; Kreibig, U. *Appl. Phys. A* **1988**, *47*, 347.

(15) Hamanaka, Y.; Nakamura, A.; Omi, S.; Del Fatti, N.; Valle, F.; Flytzanis, C. *Appl. Phys. Lett*. **1999**, *75*, 1712.

(16) (a) Roberti, T. W.; Smith, B. A.; Zhang, J. Z. *J. Chem. Phys*. **1995**, *102*, 3860. (b) Smith, B. A.; Zhang, J. Z.; Griebel, U.; Schmid, G. *Chem. Phys. Lett*. **1997**, *270*, 139.

(17) Feldstein, M. J.; Keating, K. D.; Liau, Y.-H.; Natan, M. J.; Scherer, N. F. *J. Am. Chem. Soc*. **1997**, *119*, 6638.

(18) Bloemer, M. J.; Haus, J. W.; Ashley, P. R. *J. Opt. Soc. Am. B* **1990**, *7*, 790.

(19) Wohltjen, H.; Snow, A. W. *Anal. Chem*. **1998**, *70*, 2856.

(20) Alvarez, M. M.; Khoury, J. T.; Schaff, T. G.; Shafigullia, M. N.; Vezmar, I.; Whetten, R. L. *J. Phys. Chem. B* **1997**, *101*, 3706.

(21) Kreibig, U.; Vollmer, M.; *Optical Properties of Metal Clusters*; Springer-Verlag: Berlin, 1995.

(22) Anisimov, L.; Kapeliovich, B. L.; Perelman, A. L. *Sov. Phys. JETP* **1975**, *39*, 375.

(23) Eesley, G. L. *Phys. Rev. Lett*. **1983**, *51*, 2140.

(24) Schoenlein, R. W.; Lin, W. Z.; Fujimoto, J. G.; Eesley, G. L. *Phys. Rev. Lett*. **1987**, *58*, 1680.

(25) Groeneveld, R. H. M.; Sprik, R.; Lagendijk, A. *Phys. Rev. B* **1995**, *51*, 11433.

(26) Lock, A. J.; Bakker, H. J. *J. Chem. Phys*. **2002**, *117*, 1708.

(27) Heilweil, E. J.; Casassa, M. P.; Cavanagh, R. R.; Stephenson, J. C. *J. Chem. Phys*. **1986**, *85*, 5004.

(28) Certain commercial materials and equipment are identified in this paper in order to specify adequately the experimental procedure. In no case does such an identification imply a recommendation by the National Institute of Standards and Technology nor does it imply that the material or equipment identified is necessarily the best available for this purpose.